M&C 2001 Salt Lake City, Utah, USA, September 2001.

CRITICALITY CALCULATIONS OF PROSPERO REACTOR

Christian Aussourd
Commissariat à l'Energie Atomique
BP 12
91680 Bruyères-le-Châtel
FRANCE
christian.aussourd@cea.fr

Keywords: Criticality, Deterministic, Transport, AMR, 3D

ABSTRACT

This paper demonstrates the ability, effectiveness and efficiency of the state-of-the-art AMR Deterministic code STYX to solve geometrically complex transport problems using its recently developed 3D parallel version. To do so, a CEA experimental reactor, named Prospero, mainly used for testing radiation shielding of electronic components (Zyromski et al, 1991-99), is modeled. Comparisons, against results from experiments, from the Monte Carlo Code MCNP (Briesmeister, 1997) and even from STYX 2D, are provided.

1. INTRODUCTION

The knowledge of the radiation levels, inside or around the reactor, and especially their energy and space distributions, is critical for experiments. While external measurements are easy to set up, inner remote locations remain out of reach. In this case, the only solution is to use a computer code, reliable enough to match all available tallies, and to assume it does the same everywhere. This is what we intend to do with STYX.

After a brief reminder about the main STYX features, we present the Prospero reactor and two models (2D for fast differential calculations and 3D for in depth spatial investigations). We then present the main goal of this study : estimation of the neutron energy spectrum and fluence inside the reactor knowing its power. Results are then presented and confronted with MCNP ones.

2. BACKGROUND

In 1997 we introduced STYX 2D, a tree based AMR Deterministic S_N Transport Code. This software, featuring many innovations such as an AMR rezoner and an efficient cell sorting algorithm, allows substantial cuts on running time and memory requirement. In 2000, an early 3D version (Aussourd, 2000) was presented that works on SMP architectures using MPI and OpenMP. STYX is module intensive : coarse grain with 7 satellite processes elaborating data for the main task and fine grain with ~200 ANSI C and FORTRAN 90 routines gathering more

than 35.000 source lines. The parallelization paradigm chosen so far distributes energy and angular variables over a cluster of CPUs while the geometry remains unshared. This strategy ensures a good load balancing on $N.(N+2).N_g$ processors (N being the S_N order and N_g the number of energy groups) and assumes that the whole geometry fits on one processor. Now, while a heavy parallel optimization task is underway, some real-world test cases are examined in order to validate the code and the numerical methods it uses.

3. THE PROSPERO REACTOR

Prospero is a steady 3 kW research reactor that is owned and operated by CEA. It produces neutrons and gamma rays for experimental purpose. Its twofold ^{235}U core, surrounded by a massive ^{238}U reflector, can hold small material samples for irradiation. A thick steel shroud wraps it up. Control is provided by four remote operated ^{238}U rods.

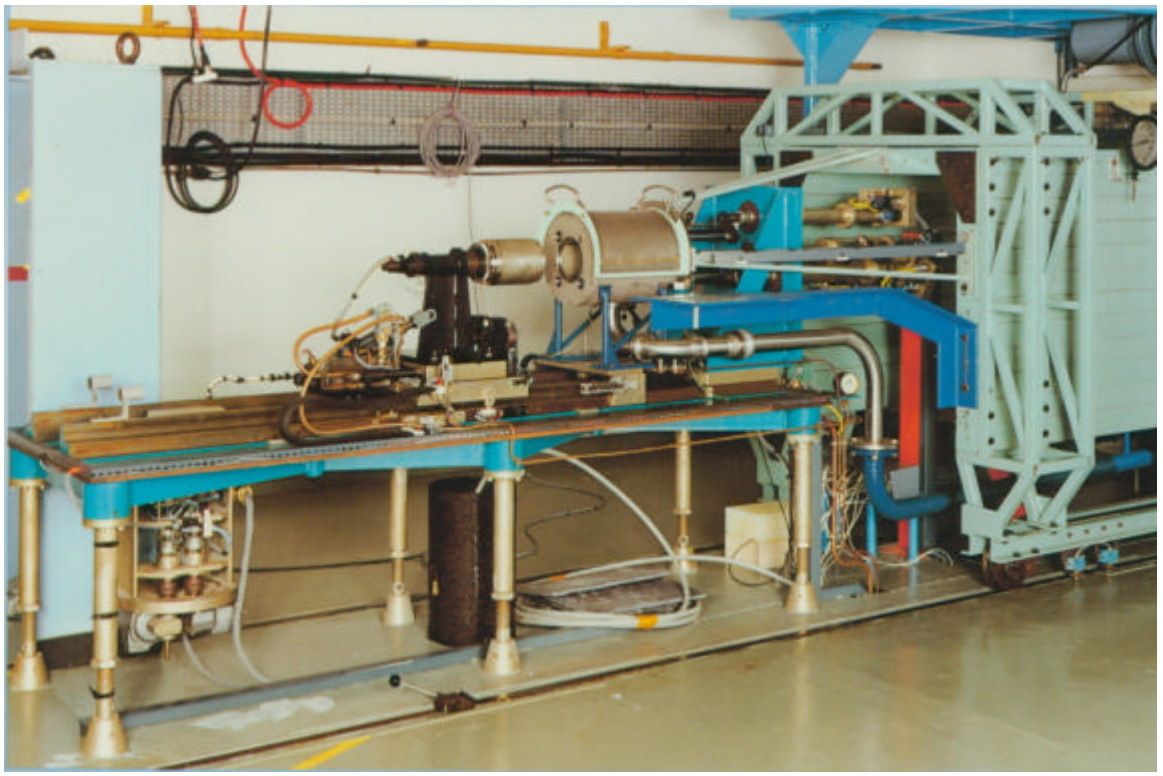

Figure 1 Prospero on Test Bed (half core extracted) – *(Photo courtesy of CEA/CVa)*

A forced cool air circulation removes decay heat from the system. This reactor, installed in a concrete bunker (Figure 1), is equipped with a fast half-core remover for security sake.

4. REACTOR MODELING

4.1 Two Dimensional Modeling

As already mentioned, Prospero is tuned with four control rods. Three of them have the same diameter and are positioned on the same circle of radius R1. They respectively occupy 50%, 62% and nearly 100% of their housings. The fourth, slimmer, is positioned at a smaller radius R2 and occupies only 20% of its housing. In order to have a faithful 2D substitute of the real 3D object, the unfilled parts of these cavities are modeled by unrolling (or spreading) them around Z axis. This approach (Figure 2 and Table 1) conserves mass and helps to preserve core activity and leakage.

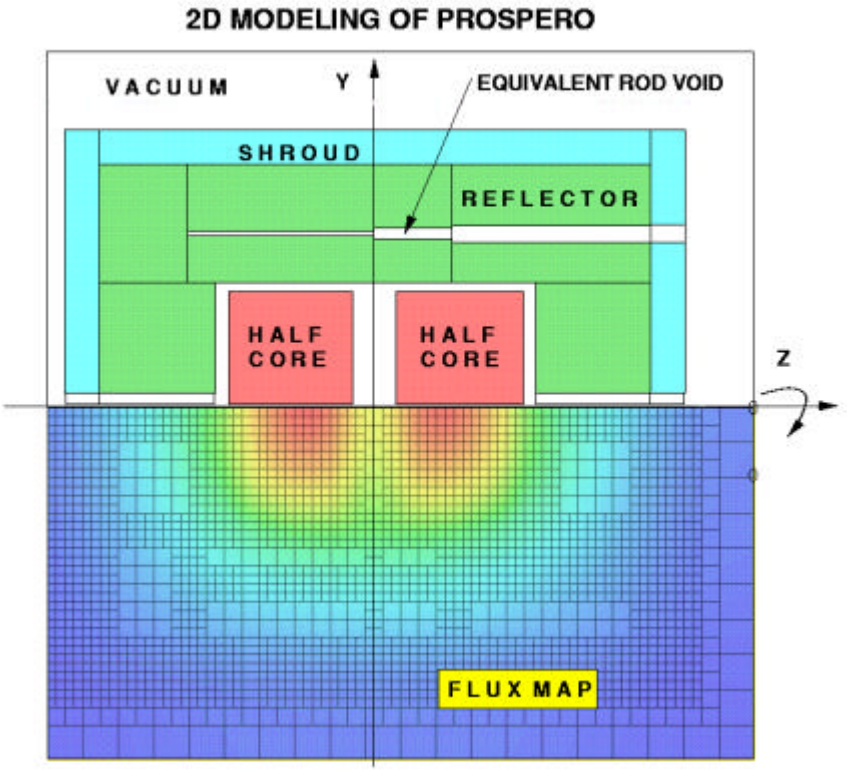

Figure 2 Two-Dimensional Modeling (flux map at the bottom)

The unrolling radius chosen, for all 4 rods, have the average value given below :

$$Re = (3.R1 + R2)/4$$

Table 1 Control rod Simulation

Distance from bottom	Event	Action
0 to 20 %	All housings full	None : Plain reflector
20 % to 50 %	Small housing empty	Unroll small housing
50 % to 62 %	One Large housing empty	Unroll (1 small + 1 large) housings
62 % to 100 %	Two more housings empty	Unroll (1 small + 3 large) housings

4.2 Three Dimensional Modeling

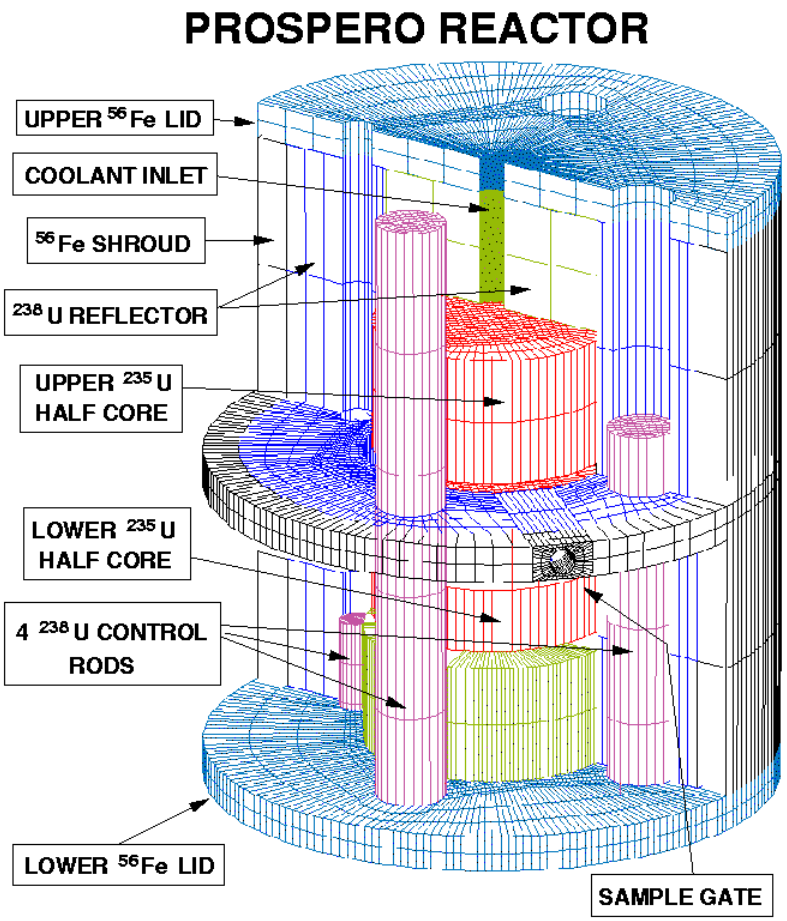

Figure 3 Inside View of the Experimental Reactor Assembly

As Prospero is a full 3D object, no symmetry can be applied, so it must be meshed as a whole. To do so we use the GIBI mesher (Axisa, 1996), part of the CEA/DMT code Castem 2000, and the Ouranos package, a CEA/DAM High Strain Rate Code (Jourdren et al,1995).

GIBI produces a hexahedron based mesh used to run a single Lagrangian time step of the Ouranos code, the result is then rezoned before to be processed by the Ouranos-Euler component that produces the Styx Cartesian input file. This strategy is quite simple to set up.

Presented in Figure 3 is the Lagrangian mesh created by GIBI. No matter how entangled or coarse it is, the Cartesian rezoner works properly because standard density objects can be fully defined by their skins.

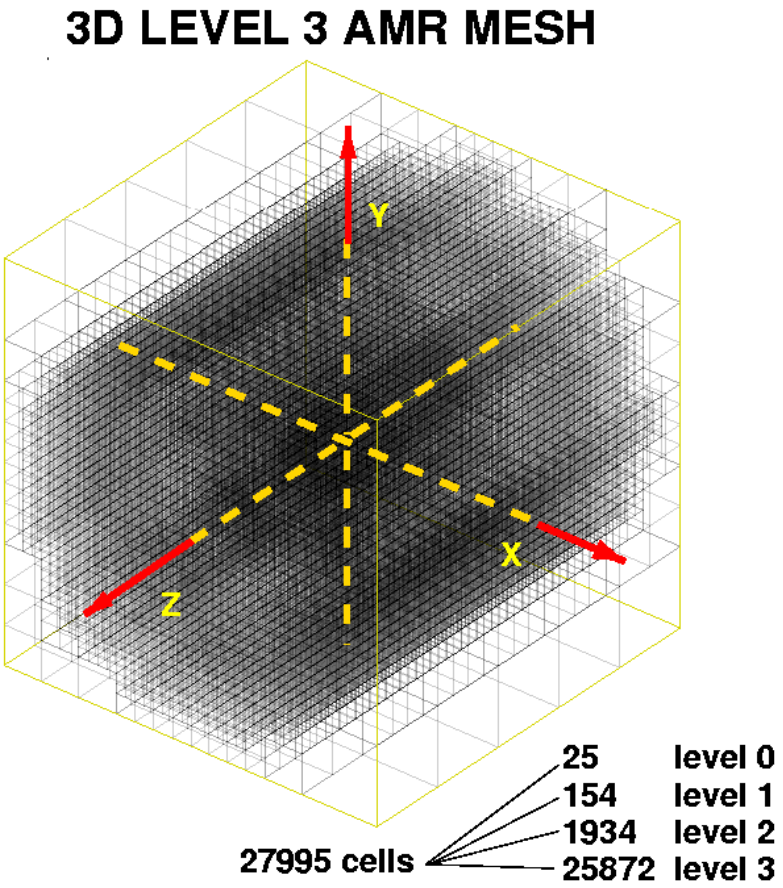

Figure 4 Level 3 AMR Mesh based on a (40x40x40) Cartesian Grid

A level 3 AMR rezoning is then applied (Figure 4) that discards 56 % of the original 64,000 Cartesian cells while preserving accuracy.

5. METHODOLOGY

5.1 Neutron Energy Spectrum at a Given Location

Let $\tilde{f}_{g,i}$ be the normalized value of $f_{g,i}$, the 1st moment of flux in the g^{th} energy group in the i^{th} cell :

$$\tilde{f}_{g,i} = \frac{f_{g,i}}{\sum_{g} f_{g,i}} \qquad (1)$$

and let ΔE_g be the width of the g^{th} group, then the g^{th} component of the energy spectrum, S can be written as :

$$S_{g,i} = \frac{\tilde{f}_{g,i}}{\Delta E_g} \qquad (2)$$

5.2 Average Energy at a Given Location

Let $\overline{E}_g$ be the mean value of the g^{th} energy group, then the average energy in the i^{th} cell can be expressed as:

$$\overline{E}_i = \sum_{g} \overline{E}_g . \tilde{f}_{g,i} \qquad (3)$$

5.3 Actual vs Computed Power

In the vicinity of criticality ($K_{eff} \approx 1$), the computed flux map (i.e. the associated eigenfunction) is representative of the actual flux map to a C multiplication factor :

$$f_{actual}(r,E) = C \, . \, f_{computed}(r,E) \qquad (4)$$

The actual power being directly proportional to the total flux :

$$\underbrace{P_{\text{actual}}}_{\text{MeV.s}^{-1}} = \frac{1}{4p} \iiint_{E,\vec{r},\vec{\Omega}} \underbrace{w_{\vec{r},E}}_{\substack{\text{energy deposit} \\ \text{MeV.cm}^{-1}}} \cdot \underbrace{f_{\vec{r},E,\vec{\Omega}}}_{\substack{\text{N.cm}^{-2} \\ .\text{s}^{-1}.\text{MeV}^{-1}}} \cdot \underbrace{dE \,.\, d^3\vec{r} \,.\, d\vec{\Omega}}_{\text{MeV.cm}^3.sr} \qquad (5)$$

is also defined to the same C multiplication factor.

Computational wise, the power expression can be derived using the macroscopic energy deposition per unit length $w_{g,i}$ in the g^{th} energy group and in the i^{th} cell :

$$w_{g,i} = N_{Avogadro} \cdot \sum_m \frac{1}{A_m} . W_{g,m} . r_{m,i} \qquad (6)$$

where $W_{g,m} = \sum_R Q^R_{g,m} . \Sigma^R_{g,m}$ is the microscopic energy deposition for element m in the g^{th} energy group and for all reactions *R*, A_m the element *m* atomic mass and $r_{m,i}$ its partial density in the i^{th} cell. The computed power can then be written as :

$$P_{computed} = \sum_g \sum_i w_{g,i} \cdot f_{g,i} . V_i \qquad (7)$$

where V_i is the volume of the i^{th} cell.

6. NUMERICAL RESULTS

This section goal consists in estimating the average neutron energy and the total fluence inside the reactor (Figure 5 - point 1) using MCNP, STYX and experimental data collected outside (Figure 5 - point 2).

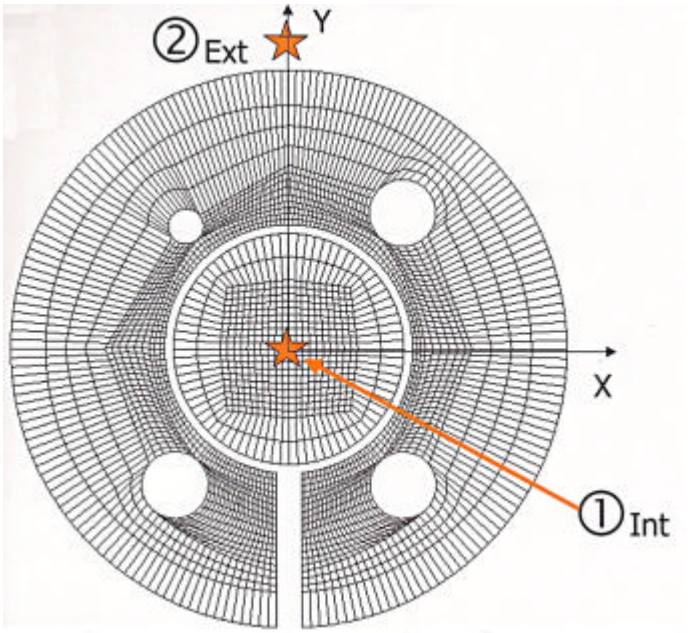

Figure 5 Probe Locations on the Equator Plane

6.1 General Information

A 32 energy group (Table 2) nuclear data set has been built based on a coarse 7 group set subdivided until convergence. The ZADIG grouper (Riz, 2000) has been used to perform this task.

Table 2 Energy Group Definition

Group #	Lower Bound (MeV)	Upper Bound (MeV)	Subdivision Count
1	0.00001	0.0001	2
2	0.0001	0.001	4
3	0.001	0.01	6
4	0.01	0.1	6
5	0.1	1.0	6
6	1.0	10.	6
7	10.	15.	2

We use the ENDF B6 Release 5 – lib 6 data base (weighted by the fission spectrum) and a P4 Anisotropic Legendre development. Prompt and delayed neutrons have been both taken into account. The unit sphere is divided into 288 angular cells using a standard S_{16} quadrature.

6.2 Global Results

Reported below (Table 3) are the experimental data and computed results by MCNP and STYX

Table 3 Experimental and Computed Data

Tally Measured and Computed	Experimental	MCNP	STYX
Power	3000 W	N/A	N/A
Total Fluence per hour (P1)	N/A	$2.83\ 10^{15}$ N.cm^{-2}	$3.15\ 10^{15}$ N.cm^{-2}
Total Fluence per hour (P2)	$1.6\ 10^{14}$ N.cm^{-2}	N/A	$1.38\ 10^{14}$ N.cm^{-2}
Average Neutron Energy (P1)	N/A	1.33 MeV	1.35 MeV
Average Neutron Energy (P2)	0.77 MeV	0.81 MeV	0.74 MeV
K_{eff}	1.00	1.0175_8 ($s = 56$ pcm)	1.0195_5

Remarks :

a) The MCNP total fluence is an estimated value resulting from the combination of the computed fluence per particle f_n and the estimated number of particles

$$\Phi_{MCNP} = f_n \cdot \underbrace{\bar{n} \cdot \frac{P_{actual}}{Q_F}}_{\text{Estimated number of particles}} \qquad (8)$$

where $\bar{n}$ is the average number of neutrons a fission produces and Q_F the energy released per fission. In counterpart, the deterministic approach used by STYX is far better because it relies on nothing but the transport theory and takes the whole reactor into account.

b) While MCNP and STYX average neutron energies are very close at point 1, they are slightly different at point 2 encircling, at ± 0.04 , the experimental value.

c) The STYX K_{eff} value is in very good agreement (less than 200 pcm) with MCNP.

d) Missing values, noted N/A, were simply not measured or computed.

6.3 Energy Spectra

In this section we estimate the neutron energy spectra in the two locations previously mentioned :

- one in center, right between the core halves,
- another on the equatorial plane opposite of the sample gate.

For both locations we compare the 2D and 3D results.

Dashed lines represent the lower and upper MCNP limits of the 95% confidence interval ($\pm 1.96\, s$).

a) Internal Probe

Confrontation between Figure 6 (2D model) and Figure 7 (3D model) confirms that no or very few 3D effects were expected at the center of the reactor, the probe being located :

- far from any rods or voids,
- in a strong fluence area dominated by fission.

There is a good agreement with MCNP. The 2D model can be used for parametric studies.

b) External Probe

Because this probe is placed in a weaker flux area just behind the steel shroud it is more prone to uncertainties. Steel with its many resonances is hard to manage, even when treated in continuous energy as MCNP did (large error bars) :

- the 3D model results are not so bad (Figure 9),
- the 2D model (Figure 8), unable to restitute 3D effects, is not recommended here for parametric studies.

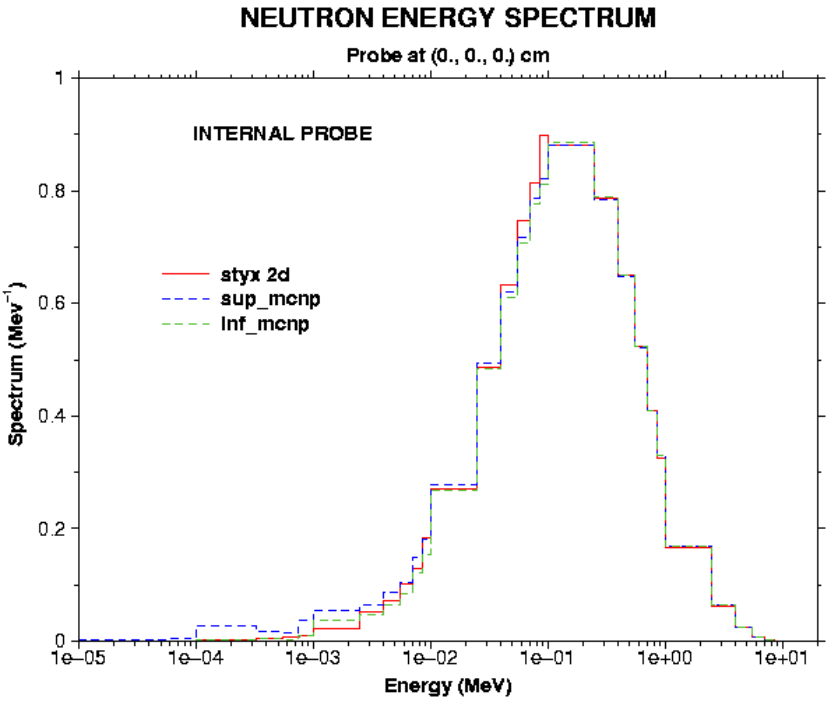

Figure 6 Energy Spectrum (Internal Probe – 2D Case)

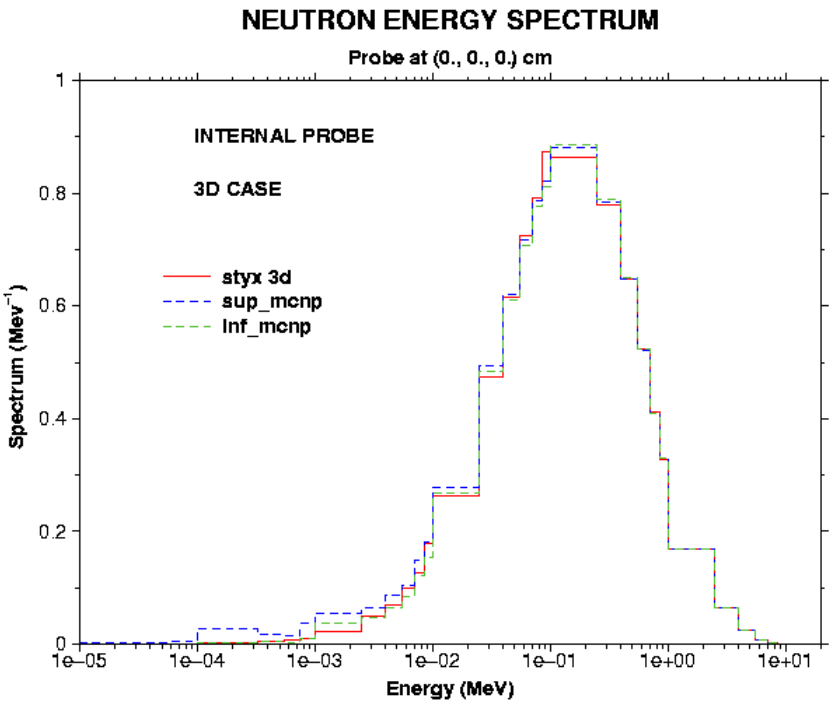

Figure 7 Energy Spectrum (Internal Probe – 3D Case)

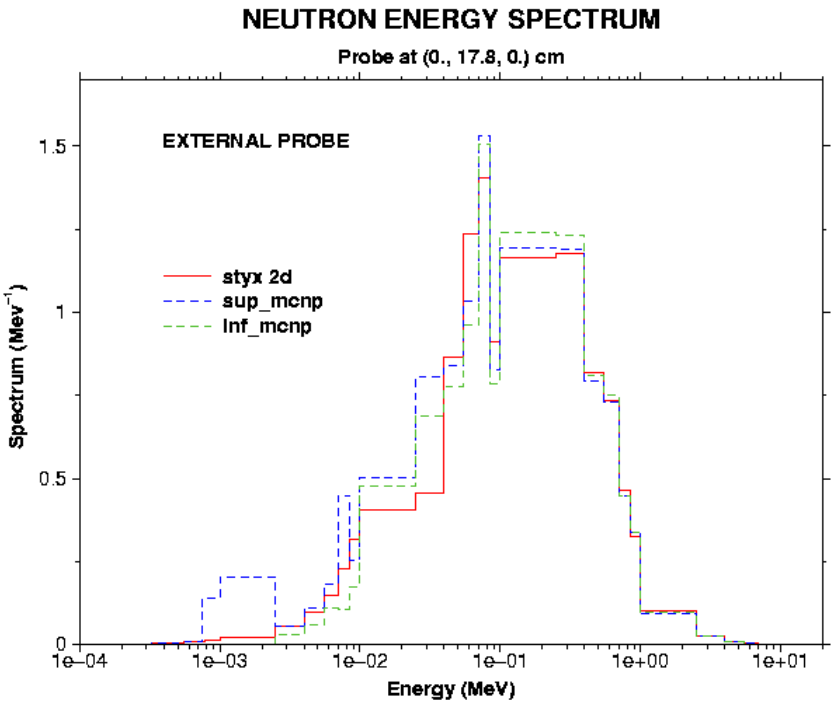

Figure 8 Energy Spectrum (External Probe – 2D Case)

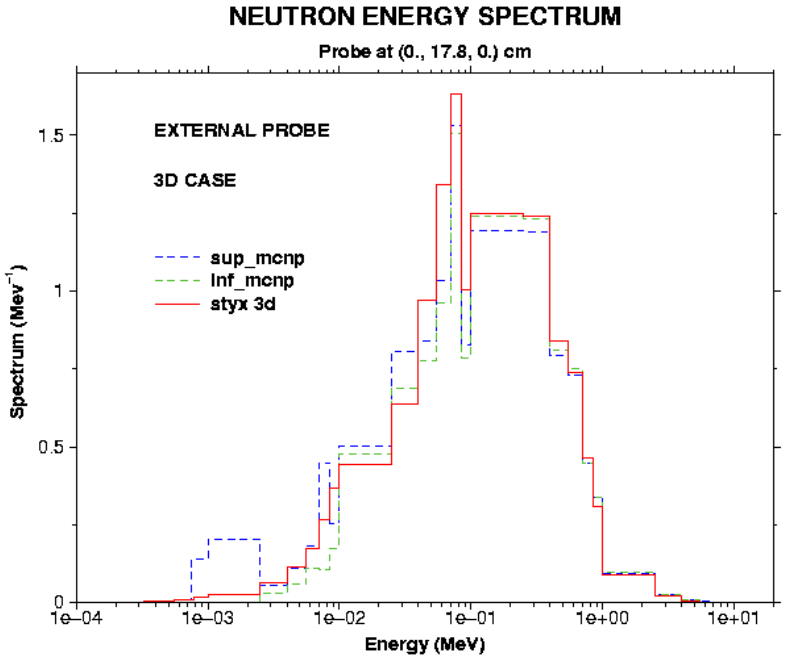

Figure 9 Energy Spectrum (External Probe – 3D Case)

6.4 Fluences and Average Energies along Equator

Presented in Figure 10 is a polar diagram of fluences and average energies collected around the Prospero equator. On the reactor outline (shaded circle), we recognize the four control rod housings and the sample gate. Next to each housing is reported the rod occupation rate for a better interpretation. The green line represents the average energies while the red one delineates the fluence variations. For both lines, a dashed circle points to the least value to ease level comparisons. Corresponding numerical data may be found in Table 4.

As we can see, the housing occupation rates significantly affect the fluences and the average energies as well. In fact, several phenomena are superimposed and compete :

1. The sparser the reflector is, the more neutrons it loses,
2. The denser the reflector is, the more the core is confined,
3. The more the core is confined, the more neutrons it produces.

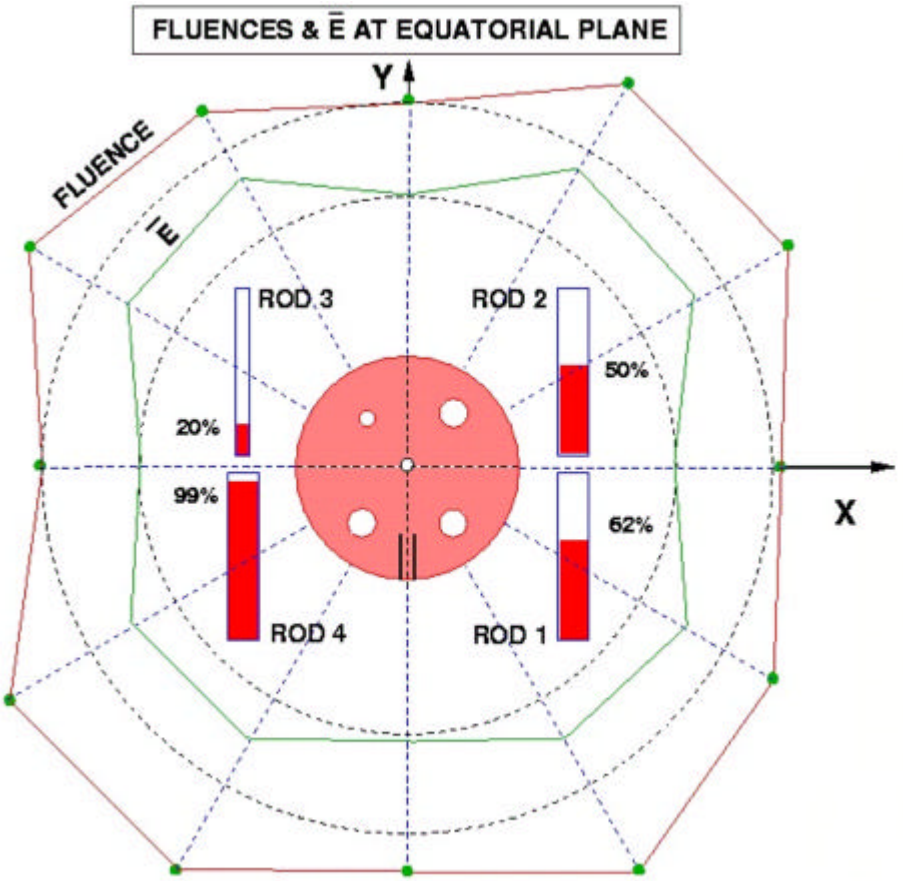

Figure 10 Measurements collected along equator

For instance, between 210° and 330°, more neutrons get out because of a greater core activity (Figure 11) induced by higher rods. The average neutron energy seems to have the same pattern as fluences for all directions.

Table 4 Fluences per hour and Average Neutron Energies along Equator

θ degrees	Fluences (10^{14}N.cm^{-2})	Average Energy (MeV)
0	1.40	0.74
30	1.72	0.92
60	1.75	0.94
90	1.38	0.74
120	1.62	0.91
150	1.76	0.88
180	1.38	0.73
210	1.86	0.87
240	1.89	0.88
270	1.55	0.77
300	1.87	0.88
330	1.64	0.90
360	1.40	0.74

6.5 Fluences along X, Y and Z axis

Presented in Figure 11 are the fluence evolutions along the three main axis.

- X and Y : have the same positive branches. It is worth noting a slight difference between their negative branches, due to a better confinement by rods # 1 and 4,

- Z, the innermost axis, bears the highest fluence; however, a saddle-like depression, due to the air-gap between the two core halves occurs near the origin.

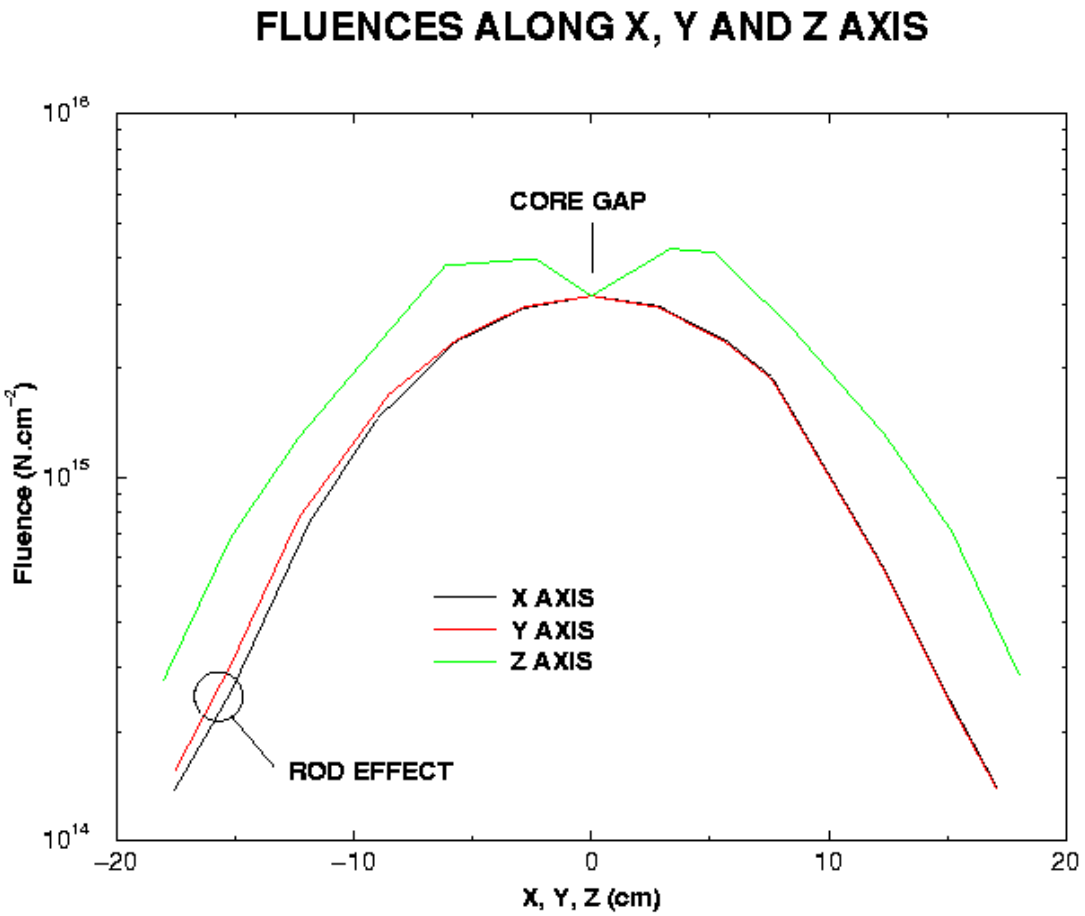

Figure 11 Fluences Along X, Y and Z Axis

6.6 Fluences along Meridians

Presented in Figure 12 are the fluence evolutions along the four main meridians : X_{min}, X_{max}, Y_{min} and Y_{max}. A noticeable rod effect, already mentioned, strengthens the fluences along the Y_{min} meridian. A rather important decrease due to rod 2 housing is recorded on X_{max} and Y_{max} meridians.

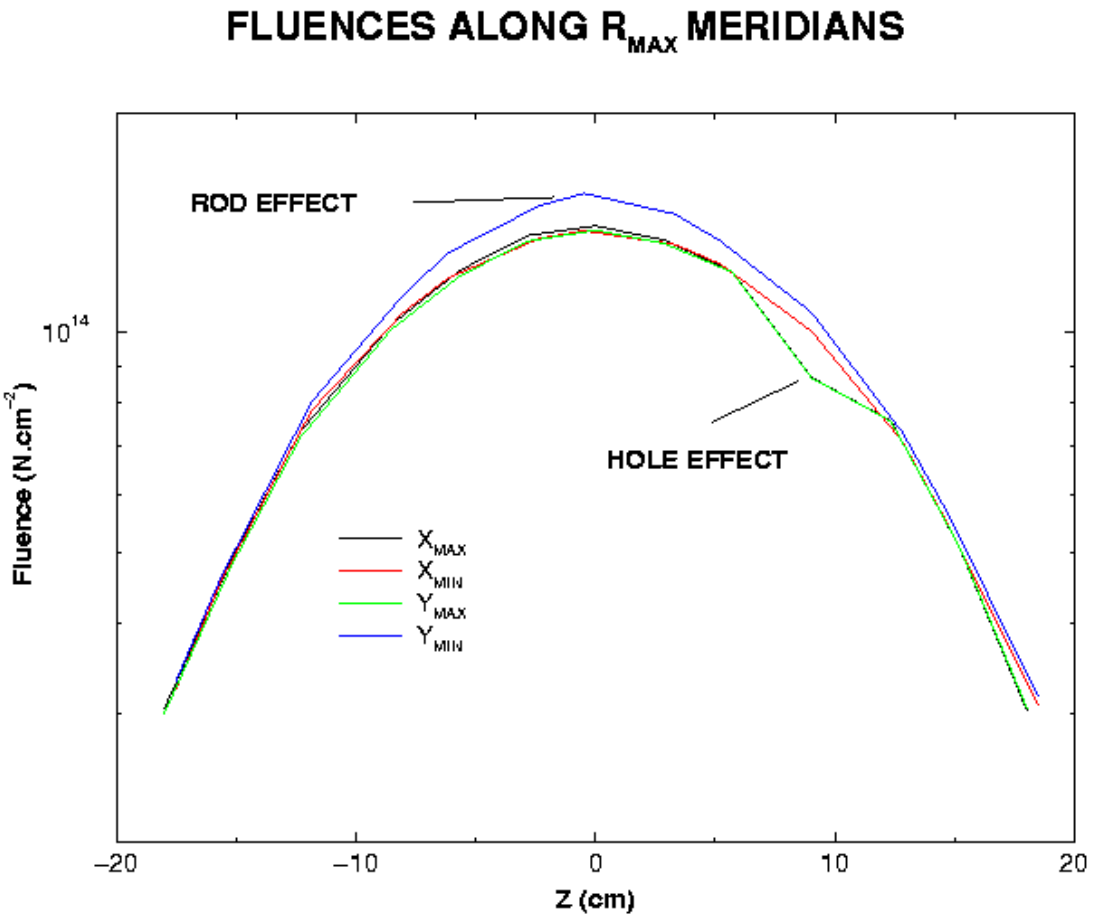

Figure 12 Fluences Along Meridians

6.7 Flux maps

Unlike Monte Carlo codes, deterministic transport codes have a complete knowledge of the phase space. For example, visually evaluating the spatial neutron distribution is as simple as a mouse click. Here (Figure 13) are represented XOY cross sections of showing the total fluences for the four leading groups (dominated by fission).

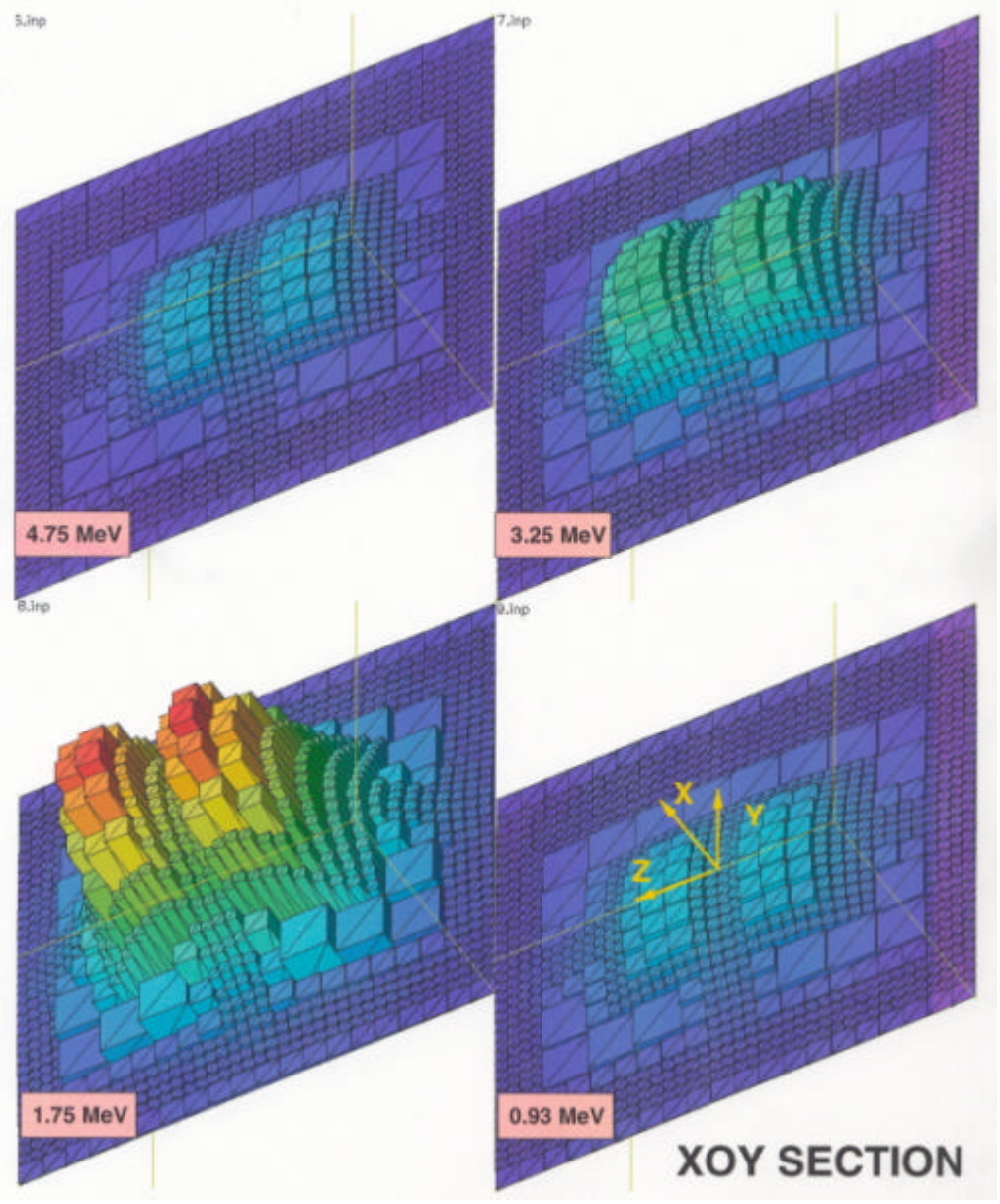

Figure 13 Fluence Map for the Most Active Energy Groups (XOY Plane)

Another useful representation is the fluence contour (Figure 14), it allows a better appreciation of 3D effects for each energy group.

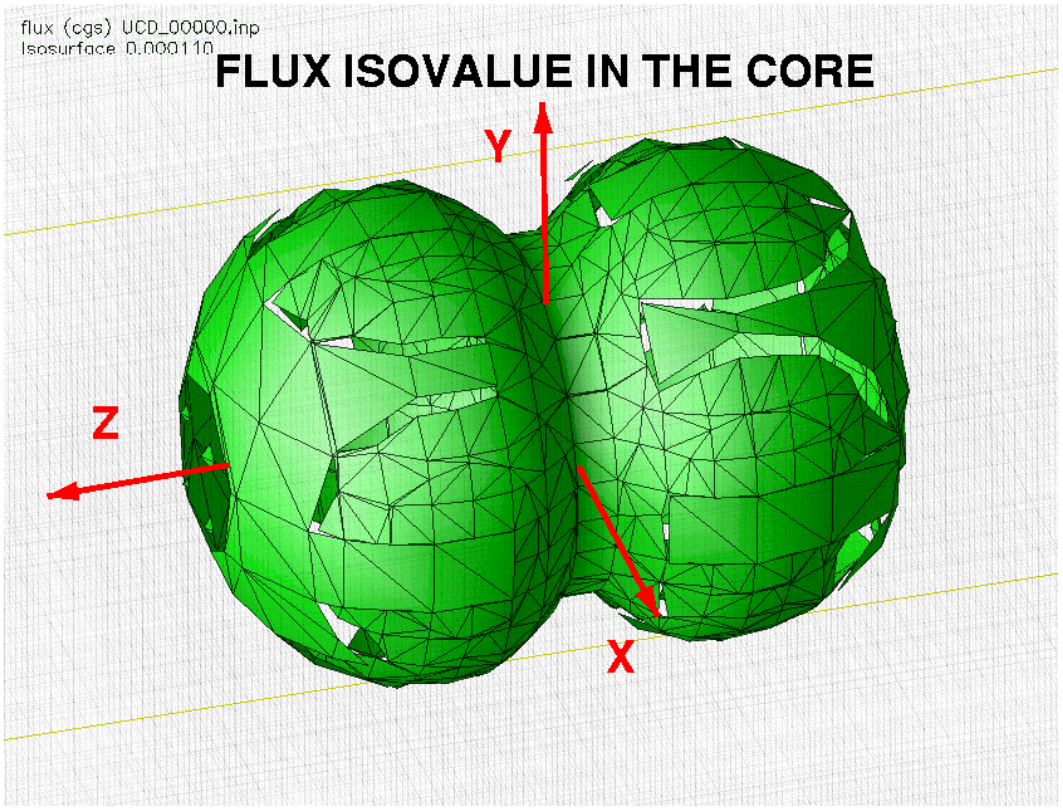

Figure 14 Fluence Isovalue

CONCLUSIONS

Our 3D AMR Deterministic Transport Code STYX has proven to be effective at reducing both run times and memory needs while preserving accuracy. A complex criticality test case has been modeled, with both 2D and 3D versions. Even with such a coarse mesh (40x40x40), it shows reasonably good agreement with the Monte Carlo Code MCNP. These results are encouraging enough to launch larger simulations.

However, beyond the careful parallel performance tuning, which is underway on our brand new Compaq SMP system, there are some prominent tasks to be done :

- Coding a restart file facility (opening the way to larger run times),
- Adding reflective boundary conditions (even though they are useless here, we need them for a lot of problems).

We confirm that for problems that fit entirely in each processor's memory, our parallelization paradigm is the best choice because of the intricacy of cell-by-cell AMR, its uneven spatial cell distribution and the trend to increase central memory.

ACKNOWLEDGMENTS

I would like to thank Augustin Umbert for his valuable MCNP results. I would also like to thank Philippe Humbert and Boukhmès Méchitoua for their assistance.

REFERENCES

Zyromski, P., Morin J., 1991-1999
RADECS European Conferences (RADiation Effects on Components and Systems)

Briesmeister, J.F, Editor, MCNP™ — A General Monte Carlo N–Particle Transport Code, Report LA–12625–M, Version 4B, Los Alamos National Laboratory, March 1997.

Aussourd, C., 2000
STYX 3D Implementation on SMP Architectures
Proceedings of Physor, ANS International Topical Meeting on Advances in Reactor Physics and Mathematics and Computation into the Next Millennium, Pittsburgh Pa, USA

Axisa, F. , 1996
CASTEM 2000 – Opérateurs Généraux de Maillage (GIBI)
Report DMT 96/498 - CEA/DRN Saclay FRANCE

Jourdren, H., Sibeaud, J.M., and Adamczewski-Cauret, M., 1995
Logiciel OURANOS : présentation et utilisation en détonique
Revue Scientifique et Technique de la Défense.

Riz, D., 2000
Calculation and Use of Multigroup Cross Sections Including Electron-Photon Cascade For a 3D Monte Carlo Neutron-Gamma Transport Code. Comparisons with MCNP-4B
Proceedings of Physor 2000, ANS International Topical Meeting on Advances in Reactor Physics and Mathematics and Computation into the Next Millennium, Pittsburgh Pa, USA,